Surface-emitting circular DFB, disk-, and ring-Bragg resonator lasers with chirped gratings: a unified theory and comparative study

Xiankai Sun[*] and Amnon Yariv

Department of Applied Physics, MC128-95, California Institute of Technology, Pasadena, CA 91125, USA
[*]Corresponding author: xksun@caltech.edu

Abstract: We have developed a theory that unifies the analysis of the modal properties of surface-emitting chirped circular grating lasers. This theory is based on solving the resonance conditions which involve two types of reflectivities of chirped circular gratings. This approach is shown to be in agreement with previous derivations which use the characteristic equations. Utilizing this unified analysis, we obtain the modal properties of circular DFB, disk-, and ring- Bragg resonator lasers. We also compare the threshold gain, single mode range, quality factor, emission efficiency, and modal area of these types of circular grating lasers. It is demonstrated that, under similar conditions, disk Bragg resonator lasers have the highest quality factor, the highest emission efficiency, and the smallest modal area, indicating their suitability in low-threshold, high-efficiency, ultracompact laser design, while ring Bragg resonator lasers have a large single mode range, high emission efficiency, and large modal area, indicating their suitability for high-efficiency, large-area, high-power applications.

OCIS codes: (250.7270) Vertical emitting lasers; (230.1480) Bragg reflectors; (050.2770) Gratings; (130.2790) Guided waves; (140.5960) Semiconductor lasers; (130.0130) Integrated optics.

References and links

1. S. A. Shakir, T. C. Salvi, and G. C. Dente, "Analysis of Grating-Coupled Surface-Emitting Lasers," Opt. Lett. **14**, 937-939 (1989).
2. D. F. Welch, R. Parke, A. Hardy, W. Streifer, and D. R. Scifres, "Low-Threshold Grating-Coupled Surface-Emitting Lasers," Appl. Phys. Lett. **55**, 813-815 (1989).
3. R. Parke, R. Waarts, D. F. Welch, A. Hardy, and W. Streifer, "High-Efficiency, High Uniformity, Grating Coupled Surface Emitting Lasers," Electron. Lett. **26**, 125-127 (1990).
4. T. Kjellberg, M. Hagberg, N. Eriksson, and A. G. Larsson, "Low-Threshold Grating-Coupled Surface-Emitting Lasers with Etch-Stop Layer for Precise Grating Positioning," IEEE Photon. Technol. Lett. **5**, 1149-1152 (1993).
5. F. S. Choa, M. H. Shih, J. Y. Fan, G. J. Simonis, P. L. Liu, T. Tanbunek, R. A. Logan, W. T. Tsang, and A. M. Sergent, "Very Low Threshold 1.55 μm Grating-Coupled Surface-Emitting Lasers for Optical Signal Processing and Interconnect," Appl. Phys. Lett. **67**, 2777-2779 (1995).
6. R. G. Waarts, "Optical Characterization of Grating Surface Emitting Semiconductor Lasers," Appl. Opt. **29**, 2718-2721 (1990).
7. T. Erdogan and D. G. Hall, "Circularly symmetric distributed feedback semiconductor lasers: An analysis," J. Appl. Phys. **68**, 1435-1444 (1990).
8. C. Wu, M. Svilans, M. Fallahi, T. Makino, J. Glinski, C. Maritan, and C. Blaauw, "Optical Pumped Surface-Emitting DFB GaInAsP/InP Lasers with Circular Grating," Electron. Lett. **27**, 1819-1821 (1991).
9. T. Erdogan, O. King, G. W. Wicks, D. G. Hall, E. H. Anderson, and M. J. Rooks, "Circularly symmetric operation of a concentric-circle-grating, surface-emitting, AlGaAs/GaAs quantum-well semiconductor laser," Appl. Phys. Lett. **60**, 1921-1923 (1992).
10. C. Wu, M. Svilans, M. Fallahi, I. Templeton, T. Makino, J. Glinski, R. Maciejko, S. I. Najafi, C. Maritan, C. Blaauw, and G. Knight, "Room temperature operation of electrically pumped Surface-Emitting Circular Grating DBR Laser," Electron. Lett. **28**, 1037-1039 (1992).
11. C. Wu, T. Makino, M. Fallahi, R. G. A. Craig, G. Knight, I. Templeton, and C. Blaauw, "Novel Circular Grating Surface-Emitting Lasers with Emission from Center," Jpn. J. Appl. Phys. **33-Pt. 2**, L427-L429 (1994).

#93647 - $15.00 USD Received 10 Mar 2008; revised 3 Jun 2008; accepted 3 Jun 2008; published 5 Jun 2008

12. R. H. Jordan, D. G. Hall, O. King, G. W. Wicks, and S. Rishton, "Lasing behavior of circular grating surface-emitting semiconductor lasers," J. Opt. Soc. Am. B **14**, 449-453 (1997).
13. C. Olson, P. L. Greene, G. W. Wicks, D. G. Hall, and S. Rishton, "High-order azimuthal spatial modes of concentric-circle-grating surface-emitting semiconductor lasers," Appl. Phys. Lett. **72**, 1284-1286 (1998).
14. K. J. Kasunic and E. M. Wright, "Nonlinear dynamics of circular-grating distributed-feedback semiconductor devices," J. Opt. Soc. Am. B **16**, 96-102 (1999).
15. A. M. Shams-Zadeh-Amiri, X. Li, and W.-P. Huang, "Above-Threshold Analysis of Second-Order Circular-Grating DFB Lasers," IEEE J. Quantum Electron. **36**, 259-267 (2000).
16. C. Bauer, H. Giessen, B. Schnabel, E.-B. Kley, C. Schmitt, and U. Scherf, "A Surface-Emitting Circular Grating Polymer Laser," Adv. Mater. **13**, 1161-1164 (2001).
17. P. L. Greene and D. G. Hall, "Effects of Radiation on Circular-Grating DFB Lasers——Part I: Coupled-Mode Equations," IEEE J. Quantum Electron. **37**, 353-364 (2001).
18. P. L. Greene and D. G. Hall, "Effects of Radiation on Circular-Grating DFB Lasers——Part II: Device and Pump-Beam Parameters," IEEE J. Quantum Electron. **37**, 364-371 (2001).
19. A. M. Shams-Zadeh-Amiri, X. Li, and W. P. Huang, "Hankel transform-domain analysis of scattered fields in multilayer planar waveguides and lasers with circular gratings," IEEE J. Quantum Electron. **39**, 1086-1098 (2003).
20. G. F. Barlow, A. Shore, G. A. Turnbull, and I. D. W. Samuel, "Design and analysis of a low-threshold polymer circular-grating distributed-feedback laser," J. Opt. Soc. Am. B **21**, 2142-2150 (2004).
21. W. M. J. Green, J. Scheuer, G. DeRose, and A. Yariv, "Vertically emitting annular Bragg lasers using polymer epitaxial transfer," Appl. Phys. Lett. **85**, 3669-3671 (2004).
22. A. Jebali, R. F. Mahrt, N. Moll, D. Erni, C. Bauer, G.-L. Bona, and W. Bachtold, "Lasing in organic circular grating structures," J. Appl. Phys. **96**, 3043-3049 (2004).
23. J. Scheuer, W. M. J. Green, G. DeRose, and A. Yariv, "Low-threshold two-dimensional annular Bragg lasers," Opt. Lett. **29**, 2641-2643 (2004).
24. J. Scheuer, W. M. J. Green, G. A. DeRose, and A. Yariv, "Lasing from a circular Bragg nanocavity with an ultrasmall modal volume," Appl. Phys. Lett. **86**, 251101 (2005).
25. G. A. Turnbull, A. Carleton, G. F. Barlow, A. Tahraouhi, T. F. Krauss, K. A. Shore, and I. D. W. Samuel, "Influence of grating characteristics on the operation of circular-grating distributed-feedback polymer lasers," J. Appl. Phys. **98**, 023105 (2005).
26. G. A. Turnbull, A. Carleton, A. Tahraouhi, T. F. Krauss, I. D. W. Samuel, G. F. Barlow, and K. A. Shore, "Effect of gain localization in circular-grating distributed feedback lasers," Appl. Phys. Lett. **87**, 201101 (2005).
27. R. Coccioli, M. Boroditsky, K. W. Kim, Y. Rahmat-Samii, and E. Yablonovitch, "Smallest possible electromagnetic mode volume in a dielectric cavity," IEE Proc.-Optoelectron. **145**, 391-397 (1998).
28. E. A. J. Marcatili, "Bends in Optical Dielectric Guides," Bell Syst. Tech. J. **48**, 2103-2132 (1969).
29. J. Scheuer and A. Yariv, "Coupled-Waves Approach to the Design and Analysis of Bragg and Photonic Crystal Annual Resonators," IEEE J. Quantum Electron. **39**, 1555-1562 (2003).
30. J. Scheuer and A. Yariv, "Annular Bragg defect mode resonators," J. Opt. Soc. Am. B **20**, 2285-2291 (2003).
31. X. K. Sun, J. Scheuer, and A. Yariv, "Optimal design and reduced threshold in vertically emitting circular Bragg disk resonator lasers," IEEE J. Sel. Top. Quantum Electron. **13**, 359-366 (2007).
32. X. K. Sun and A. Yariv, "Modal properties and modal control in vertically emitting annular Bragg lasers," Opt. Express **15**, 17323-17333 (2007).
33. R. F. Kazarinov and C. H. Henry, "Second-Order Distributed Feedback Lasers with Mode Selection Provided by First-Order Radiation Losses," IEEE J. Quantum Electron. **QE-21**, 144-150 (1985).
34. A. Jebali, D. Erni, S. Gulde, R. F. Mahrt, and W. Bachtold, "Analytical calculation of the *Q* factor for circular-grating microcavities," J. Opt. Soc. Am. B **24**, 906-915 (2007).

1. Introduction

Grating coupled surface emitting lasers have attracted considerable attention over the past decade due to features such as single-mode operation and the potential for on-chip 2D laser array integration with applications in coherent beam combination [1-6]. Among the various grating coupled schemes, circular grating lasers with large emission apertures possess the additional advantage of producing circularly-symmetric, narrow-divergence laser beams, making them convenient for coupling to fibers [7-26]. In such lasers, the grating serves two purposes: confining the in-plane fields to form a radial resonator and secondly acting as a broadside output coupler. Due to the inherent high values of Q/V (Q, quality factor of resonator mode; V, modal volume), these resonators are excellent candidates for low-threshold, single-mode operation taking advantage of the large Purcell effect [27].

In conventional circular resonators, Q and V are related due to the "bending loss" problem where smaller radii lead to increased radiation losses [28]. To break this linkage, we proposed a novel type of annular resonator based on radial Bragg reflection [29, 30]. Devices

#93647 - $15.00 USD Received 10 Mar 2008; revised 3 Jun 2008; accepted 3 Jun 2008; published 5 Jun 2008

implementing this design have demonstrated both a low threshold and a small modal volume [23, 24]. A comprehensive coupled-mode theory, including the effects of vertical radiation, on the threshold gain and emission efficiency of such circular grating lasers has been derived and used for analyzing disk type Bragg resonator lasers [31] and ring type Bragg resonator lasers [32]. The threshold gains were obtained by solving characteristic equations. However, the complexity of the characteristic equations rendered them difficult to analyze and interpret intuitively. Moreover, though the circular DFB, disk-, and ring- Bragg resonator lasers all belong to the family of circular grating lasers, they were not comparable because the analyses used to treat them were not directly related. In this paper we present a unified analysis and discussion of the aforementioned types of circular grating lasers, and compare the threshold gain, single mode range, quality factor, emission efficiency, and modal area, of these devices.

This paper is structured in the following manner: In Section 2, the coupled-wave equations are solved obtaining two different reflectivities for the chirped circular Bragg gratings under two typical boundary conditions of circular geometry. In Section 3, the two types of reflectivities are employed to derive the resonance conditions, with which the resonant modes of circular DFB, disk-, and ring- Bragg resonator lasers are then numerically obtained. In Section 4, the threshold gains, single mode ranges, quality factors, emission efficiencies, and modal areas of these structures are calculated, compared, and discussed. Section 5 is a summary of these results.

2. Reflectivities of chirped circular Bragg gratings

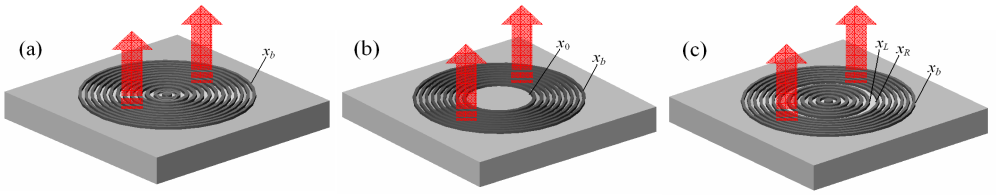

Fig. 1. Illustration of chirped circular grating lasers: (a) Circular DFB laser; (b) Disk Bragg resonator laser; (c) Ring Bragg resonator laser. Laser radiation is coupled out of the resonators in vertical direction via the gratings.

Shown in Fig. 1 are three configurations of circular grating lasers: (a) Circular DFB lasers, in which the grating extends from the center to the exterior boundary x_b. (b) Disk Bragg resonator lasers, in which a center disk is surrounded by a radial Bragg grating extending from x_0 to x_b. (c) Ring Bragg resonator lasers, in which a circumferential defect is surrounded by inner and outer gratings on both sides. The inner grating extends from the center to x_L while the outer from x_R to x_b. As detailed in [29] and [30], in order to optimally interact with the optical fields, the gratings have to be designed to match the phase of the modal fields. The eigenmodes of the wave equation in cylindrical coordinates, the Bessel functions, have nonperiodic zeros, yielding a radial chirp modulation of the refractive index, i.e., chirped gratings.

In [31] we derived a comprehensive coupled-mode theory, by including the effect of resonant vertical radiation, to analyze such chirped circular grating structures in active media. Using the Green's function method, the effect of vertical radiation is incorporated into the coupled in-plane wave equations, and a set of evolution equations for the amplitudes of the in-plane waves is obtained:

$$\begin{cases} \dfrac{dA}{dx} = uA - vBe^{2i\delta \cdot x} \\ \dfrac{dB}{dx} = -uB + vAe^{-2i\delta \cdot x} \end{cases} \tag{1}$$

where A and B are the amplitudes of the in-plane outward- and inward- propagating cylindrical waves, respectively. x is the normalized radius $x=\beta\rho$. $\delta=(\beta_{\text{design}}-\beta)/\beta$ denotes the

#93647 - $15.00 USD Received 10 Mar 2008; revised 3 Jun 2008; accepted 3 Jun 2008; published 5 Jun 2008

normalized frequency detuning factor. The coefficients u and v are defined as $u=g_A-h_1$, $v=h_1+ih_2$, where g_A is the normalized gain coefficient. The minimum value of g_A required to achieve laser emission will be determined by the resonance condition. h_1 and h_2 are the radiation- and feedback- coupling coefficients, respectively. It should be noted that, although Eqs. (1) seem to be a set of coupled equations for in-plane (vertically confined) waves only, they implicitly include the effect of vertical radiation due to h_1. In terms of obtaining the threshold for the lasing modes, vertical radiation is treated as a loss term.

To solve for A and B, $\tilde{A}=Ae^{-i\delta x}$ and $\tilde{B}=Be^{i\delta x}$ are introduced, and (1) becomes

$$\begin{cases} \dfrac{d\tilde{A}}{dx}=(u-i\delta)\tilde{A}-v\tilde{B} \\ \dfrac{d\tilde{B}}{dx}=-(u-i\delta)\tilde{B}+v\tilde{A} \end{cases} \tag{2}$$

the generic solutions of which are

$$\begin{cases} \tilde{A}(x)=\tilde{A}(0)\dfrac{\sinh[S(x-L)]+\mathbb{C}\cosh[S(x-L)]}{-\sinh[SL]+\mathbb{C}\cosh[SL]} \\ \tilde{B}(x)=\dfrac{\tilde{A}(0)}{v}\dfrac{[(u-i\delta)-\mathbb{C}S]\sinh[S(x-L)]+[\mathbb{C}(u-i\delta)-S]\cosh[S(x-L)]}{-\sinh[SL]+\mathbb{C}\cosh[SL]} \end{cases} \tag{3}$$

where S is defined as $S=\sqrt{(u-i\delta)^2-v^2}$, $\mathbb{C}$ is a constant to be determined by specific boundary conditions, and L is a normalized length parameter.

Next we consider two types of boundary conditions to obtain the field reflectivity in each case.

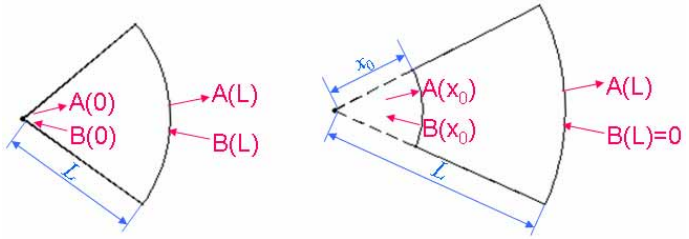

Fig. 2. Illustration of the two types of boundary conditions for calculating reflectivities. Left: $A(0)=B(0)$, $r_1(L)=A(L)/B(L)$; Right: $B(L)=0$, $r_2(L,x_0)=B(x_0)/A(x_0)$.

1. The grating extends from the center $x=0$ to $x=L$. An inward propagating wave with amplitude $B(L)$ impinges from outside on the grating.

We have to ensure at the center $A(0)=B(0)$, $\tilde{A}(0)=\tilde{B}(0)$, leading to $\mathbb{C}=\frac{(u-v-i\delta)\sinh[SL]+S\cosh[SL]}{S\sinh[SL]+(u-v-i\delta)\cosh[SL]}$ and to the reflectivity

$$r_1(L)=\frac{A(L)}{B(L)}=\frac{\tilde{A}(L)e^{i\delta L}}{\tilde{B}(L)e^{-i\delta L}}=e^{2i\delta L}\frac{(u-v-i\delta)\sinh[SL]+S\cosh[SL]}{-(u-v-i\delta)\sinh[SL]+S\cosh[SL]}. \tag{4}$$

2. The grating extends from $x=x_0$ to $x=L$. An outward propagating wave with amplitude $A(x_0)$ impinges from inside on the grating.

Since there is no inward propagating wave coming from outside, we invoke $B(L)=0$, $\tilde{B}(L)=0$, leading to $\mathbb{C}=\frac{S}{u-i\delta}$ and to the reflectivity

$$r_2(x_0,L)=\frac{B(x_0)}{A(x_0)}=\frac{\tilde{B}(x_0)e^{-i\delta x_0}}{\tilde{A}(x_0)e^{i\delta x_0}}=e^{-2i\delta x_0}\frac{v\sinh[S(L-x_0)]}{(u-i\delta)\sinh[S(L-x_0)]-S\cosh[S(L-x_0)]}. \tag{5}$$

#93647 - $15.00 USD Received 10 Mar 2008; revised 3 Jun 2008; accepted 3 Jun 2008; published 5 Jun 2008

It is worth noting that, as seen from their definitions, the above reflectivities include the propagation phase.

As a case study, we take the specific coupling coefficients h_1=0.0072+0.0108i and h_2=0.0601 of a quarter-duty-cycle Hankel-phased rectangular grating from previous work [31]. The two reflectivities (4) and (5) in the cases where the normalized grating length ($\beta\Delta\rho$) is 100 are analyzed. Their amplitudes $|r_1(100)|$ and $|r_2(x_0,x_0+100)|$ are plotted in Fig. 3 with different gain levels.

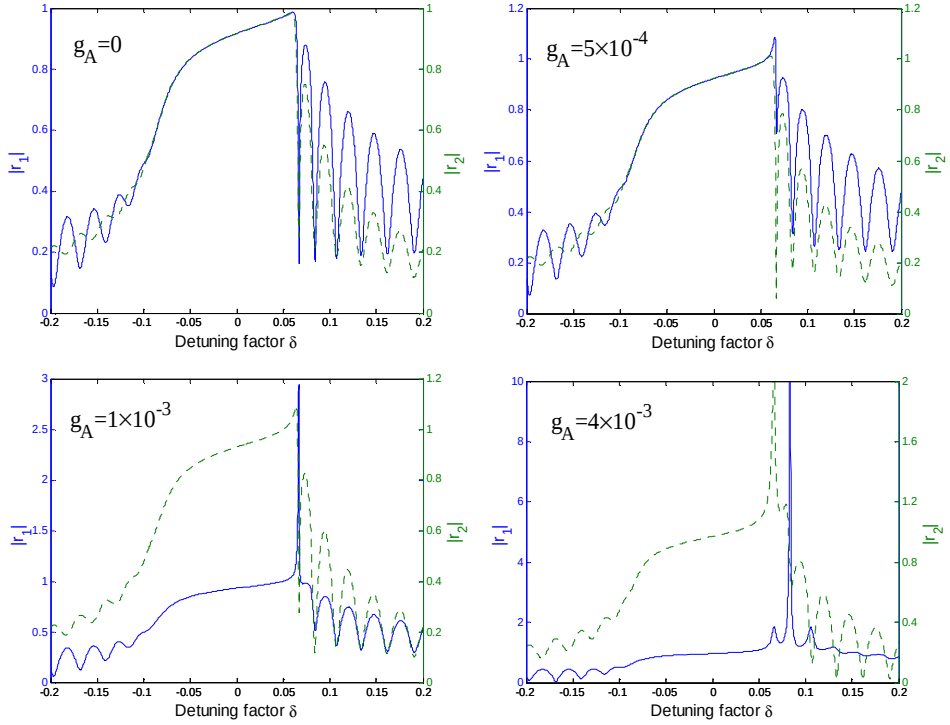

Fig. 3. Reflectivities $|r_1(100)|$ and $|r_2(x_0,x_0+100)|$ for different gain levels g_A=0, 5×10^{-4}, 1×10^{-3}, and 4×10^{-3}, in the presence of vertical radiation.

For the passive case (g_A=0), there exists a high reflection region at the center (–0.06 <δ<0.06), corresponding to the band gap of the Bragg gratings. As the gain (g_A) increases, both $|r_1|$ and $|r_2|$ grow and exceed unity first at one bandgap edge. Further increases in gain result in the existence of more lobes with peak value greater than unity. Additionally, both $|r_1|$ and $|r_2|$ are asymmetric with respect to δ=0. The fringes with positive δ have more pronounced oscillations than those with negative δ. This mode selection is attributed to the involvement of vertical radiation coupling. Similar to the case of a linear second-order Bragg grating, the radiation fields coupled out from the outward and inward in-plane cylindrical waves interfere constructively at one bandgap edge and destructively at the other. The destructive interference of radiation fields at one of the bandgap edges is the mode selection mechanism [33]. Engineering of this modal selection method is key to designing high-efficiency single-mode ring Bragg resonator lasers [32].

3. Resonance conditions for circular DFB, disk-, and ring- Bragg resonator lasers

Utilizing the reflectivities for different boundary conditions, it is possible to derive the resonance conditions for each circular grating laser configuration.

In circular DFB lasers, the limiting cases $r_1(x_b)\rightarrow\infty$ or $r_2(0,x_b)$=1 lead to

$$\tanh[Sx_b]=\frac{S}{u-v-i\delta}. \tag{6}$$

#93647 - $15.00 USD Received 10 Mar 2008; revised 3 Jun 2008; accepted 3 Jun 2008; published 5 Jun 2008

Disk Bragg resonator lasers have reflectivity equal to unity at the center so that the resonance condition is $1 \cdot e^{2g_A x_0} \cdot r_2(x_0, x_b) = 1$, which reads

$$e^{2(g_A - i\delta)x_0} \frac{v \sinh[S(x_b - x_0)]}{(u - i\delta)\sinh[S(x_b - x_0)] - S\cosh[S(x_b - x_0)]} = 1. \quad (7)$$

The resonance condition of ring Bragg resonator lasers is $r_1(x_L) \cdot e^{2g_A(x_R - x_L)} \cdot r_2(x_R, x_b) = 1$, which reads

$$e^{2(g_A - i\delta)(x_R - x_L)} \frac{(u - v - i\delta)\sinh[Sx_L] + S\cosh[Sx_L]}{-(u - v - i\delta)\sinh[Sx_L] + S\cosh[Sx_L]} \cdot \frac{v \sinh[S(x_b - x_R)]}{(u - i\delta)\sinh[S(x_b - x_R)] - S\cosh[S(x_b - x_R)]} = 1. \quad (8)$$

Though in much simpler forms, the above resonance conditions are essentially the same as those characteristic equations derived in Refs. [31] and [32]. The foundation for validity of the "resonance condition theory" is the continuity of the amplitudes of the cylindrical waves at the interfaces. The in-plane electric field is expressed as $E(x) = A(x)H_m^{(1)}(x) + B(x)H_m^{(2)}(x)$. The continuity conditions for the outward and inward propagating waves require that $A(x_0^-) = A(x_0^+)$ and $B(x_0^-) = B(x_0^+)$ hold at *any* interface x_0. They adequately guarantee the continuity of the in-plane electric field and its first derivative, which are the only requirements for matching the fields at the interfaces in deriving the characteristic equations. The restrictions at the center and exterior boundary are automatically satisfied by choosing proper reflectivities. Therefore, using the resonance condition theory, we simplify and unify the derivation of threshold conditions for the family of circular grating coupled surface emitting lasers.

Table 1. Modal threshold gains (g_A), frequency detuning factors (δ), and modal fields of the circular DFB, disk-, and ring- Bragg resonator lasers (x_b = 200).

Mode number		1	2	3	4	5
Circular DFB laser	g_A (10^{-3})	0.283	1.03	2.04	3.11	4.12
	δ (10^{-3})	61.8	66.6	74.1	83.6	94.6
	Modal field	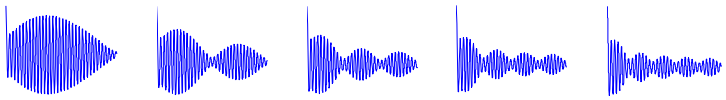				
Disk Bragg resonator laser	g_A (10^{-3})	0.127	0.288	0.454	0.690	1.21
	δ (10^{-3})	49.8	21.2	–8.09	–37.4	–66.5
	Modal field	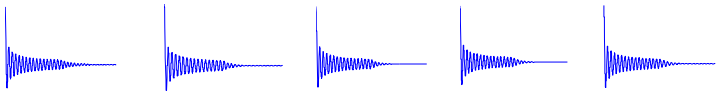				
Ring Bragg resonator laser	g_A (10^{-3})	0.457	1.06	1.92	3.14	4.09
	δ (10^{-3})	55.9	66.9	71.0	84.4	91.6
	Modal field	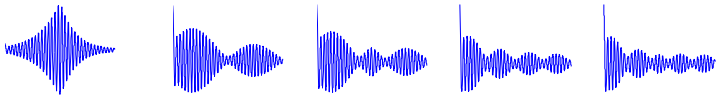				

To compare the modal properties of the circular DFB, disk-, and ring- Bragg resonator lasers, we adopt a typical device size for such lasers with an exterior boundary radius

#93647 - $15.00 USD Received 10 Mar 2008; revised 3 Jun 2008; accepted 3 Jun 2008; published 5 Jun 2008

ρ_b=17.5μm ($x_b=\beta\rho_b\approx$200) used in [23]. For the disk Bragg resonator laser, the inner disk radius is set to be $x_0=x_b/2$=100. For the ring Bragg resonator laser, the annular defect is assumed to be located at the middle $x_b/2$, with its width being a wavelength of the cylindrical waves therein, so that $x_L+x_R=x_b$=200, $x_R-x_L=2\pi$. Introducing all these parameters, along with the coupling coefficients h_1 and h_2, into each resonance condition (6), (7), and (8) produces information about the modes of each structure. The results for the 5 lowest-order modes are listed in Table 1.

The following is a comparison of the modal properties of the three laser structures. All 5 modes of the circular DFB laser are in-band modes on one side of the band gap. This is due to the aforementioned radiation-coupling-induced mode selection mechanism. Increased gain results in the excitation of higher-order modes. All the displayed modes of the disk Bragg resonator laser are confined to the center disk with negligible peripheral power leakage and thus possess very low thresholds and very small modal volumes. The modes of the ring Bragg resonator laser, with the exception of the lowest-order defect mode, all resemble their counterparts in the circular DFB case. The defect mode has a larger threshold gain than the first mode of the circular DFB device, however it possesses a much higher emission efficiency as will be subsequently shown.

4. Single mode range, quality factor, emission efficiency, and modal area for circular DFB, disk-, and ring- Bragg resonator lasers

4.1 Single mode range

Generally, larger devices with longer radial Bragg gratings are able to achieve lower threshold gain levels though these devices suffer from smaller modal discrimination. There exists a range of the exterior boundary radius x_b values for which single mode operation in each laser configuration can be achieved. This range is referred to as the "single mode range." Similar to the prior calculations with a fixed x_b, once again, for the disk Bragg resonator lasers, the inner disk radius is set to be $x_0=x_b/2$, while for the ring Bragg resonator lasers, the annular defect is assumed to be located at the middle $x_b/2$, with the width being a cylindrical wavelength ($x_L+x_R=x_b$, $x_R-x_L=2\pi$). Figure 4 plots the evolution of threshold gains for the 5 lowest-order modes as x_b varies from 50 to 350. The single mode ranges for circular DFB, disk-, and ring-Bragg resonator lasers are 50–250, 60–140, and 50–250, respectively. Since single mode operation is usually preferred in laser designs, in what follows we limit x_b to remain within each single mode range and focus our discussion on the first lasing mode only.

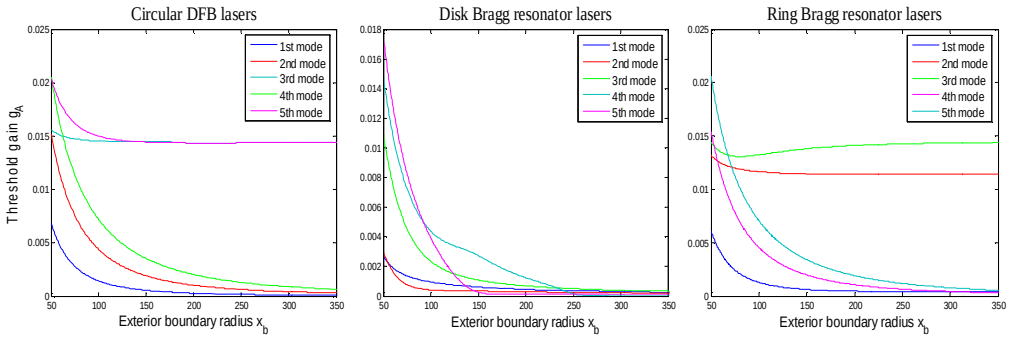

Fig. 4. Evolution of threshold gains of the 5 lowest-order modes of circular DFB, disk-, and ring- Bragg resonator lasers.

4.2 Quality factor

The quality factor Q for optical resonators is usually defined as $\frac{\omega\mathcal{E}}{P}$ where ω denotes the radian resonance frequency, $\mathcal{E}$ the total energy stored in the resonator, and P the power loss. The quality factor is a measure of the speed with which a resonator dissipates its energy. In

#93647 - $15.00 USD Received 10 Mar 2008; revised 3 Jun 2008; accepted 3 Jun 2008; published 5 Jun 2008

the circular grating lasers investigated here, the power loss P has two contributions: vertical radiation coupled out of the resonator due to the first-order Bragg diffraction, and peripheral leakage due to the finite radial length of the Bragg reflector.

Jebali *et al*. recently developed an analytical formalism to calculate the Q factor for first-order circular grating resonators in a 2D configuration [34]. Due to the 2D aspect of their model, only in-plane peripheral leakage was considered as the source of power loss. Here we study a 3D case and include vertical radiation in the power loss. Nevertheless, we do not plan to derive an exact expression for Q. Rather, by considering that the energy stored in a volume is proportional to $\int |\mathbf{E}|^2 \, dV$ and that the outflow power through a surface is proportional to $\int |\mathbf{E}|^2 \, dS$, we define an unnormalized quality factor

$$Q' = \frac{\int_0^D dz \int_0^{2\pi} d\varphi \int_0^{\rho_b} |E(\rho,z)|^2 \, \rho d\rho}{\iint\limits_{grating} |\Delta E(\rho, z=0)|^2 \, \rho d\rho d\varphi + \int_0^D dz \int_0^{2\pi} |E(\rho=\rho_b, z)|^2 \, \rho_b d\varphi} = \frac{\int_0^D Z^2(z)dz \cdot \int_0^{x_b} |E(x)|^2 \, x dx}{\int\limits_{grating} |\Delta E(x, z=0)|^2 \, x dx + \int_0^D Z^2(z)dz \cdot |E(x=x_b)|^2 \, \beta x_b} \tag{9}$$

where $Z(z)$ denotes the vertical mode profile for the layer structure and D the thickness of the resonator. Due to the angular symmetry (for m=0 under consideration), the angular integration factors are canceled out. Detailed expressions for the in-plane field E and radiated field ΔE can be found in [31]. To within a scaling factor, the unnormalized quality factor Q' is essentially the same as the usually defined Q, however it is more intuitive and convenient for calculational purposes. The results of our calculations for the unnormalized quality factor for each laser configuration are displayed in Fig. 5. As expected, increases in the device size (x_b) resulted in an enhanced Q' value. Additionally, the disk Bragg resonator lasers exhibited a much higher Q' than the other laser structures of identical dimensions. As an example, for x_b=100, the Q' value of the disk Bragg resonator device is approximately 3 times greater than that of the circular DFB or ring Bragg resonator structures. This is in agreement with their lower-threshold behavior shown in Table 1.

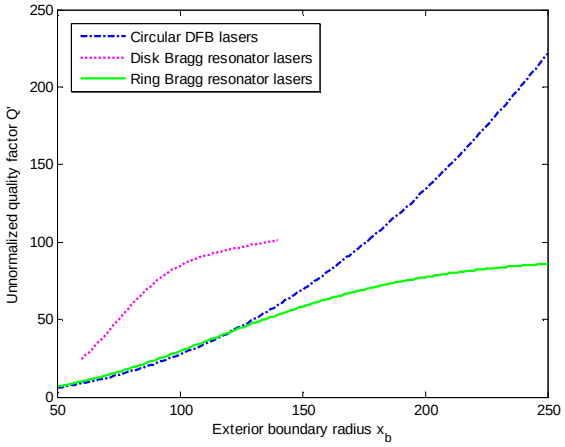

Fig. 5. Unnormalized quality factors of circular DFB, disk-, and ring- Bragg resonator lasers.

4.3 Emission efficiency

It is natural to define the emission efficiency η as the fraction of the total power loss which is represented by the useful vertical radiation. Figure 6 depicts the η of the first lasing modes, within each single mode range, for each device structure. As expected, all the lasers possess a

#93647 - $15.00 USD Received 10 Mar 2008; revised 3 Jun 2008; accepted 3 Jun 2008; published 5 Jun 2008

larger η with a larger device size. Comparing devices of identical dimensions, only the disk- and ring- Bragg resonator lasers achieve high emission efficiencies. This is a result of the first lasing modes of these structures being bandgap modes while the first lasing mode of the circular DFB laser is a bandgap-edge (in-band) mode. Bandgap modes experience much stronger reflection from the Bragg gratings, yielding less peripheral power leakage than in-band modes.

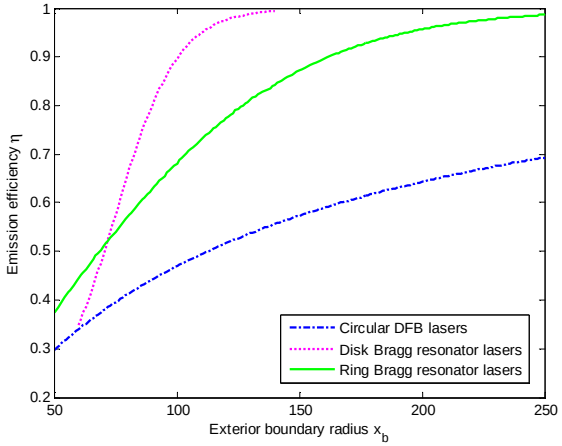

Fig. 6. Emission efficiencies of circular DFB, disk-, and ring- Bragg resonator lasers.

4.4 Modal area

Based on the usual definition of modal volume [27], we define an effective modal area as $A_{mode}^{eff} = \frac{\iint |\mathbf{E}|^2 \, x dx d\varphi}{\max\{|\mathbf{E}|^2\}}$. The modal area is a measure of how the modal field is distributed within the resonator. A highly localized field can have a small modal area and therefore strong interaction with the emitter. Figure 7 is a plot of A_{mode}^{eff} of the first lasing modes, within each single mode range, for each structure type. As a reference, the top surface area of the devices (πx_b^2) is also plotted. The modal area of the disk Bragg resonator lasers was found to be at least one order of magnitude lower than those of the circular DFB and ring Bragg resonator lasers. This is not surprising and can be inferred from their unique modal profiles listed in Table 1. Furthermore, our previous work has demonstrated single-mode lasing with ultrasmall modal volume in a nanosized disk Bragg resonator in InGaAsP quantum well active membrane [24]. Clearly, a disk configuration is preferable in ultracompact laser design. Alternatively, ring Bragg resonator lasers have a large modal area with high emission efficiency, rendering them suitable for high-efficiency, high-power, large-area laser applications.

Figure 7 illustrates a turning point for ring Bragg resonator lasers at x_b=113 beyond which the curve becomes oscillatory. This is due to the switching of the maximal value of |**E**| in the denominator of A_{mode}^{eff}. Figure 8 shows that for x_b<113 the field at the center dominates, while for x_b>113 the field at the defect dominates. The oscillation of the peak value at the defect (as x_b varies) reflects on the results of the modal area. Circular DFB and disk Bragg resonator lasers do not exhibit this behavior because the maximal |**E**| of these structures is always located at the center.

#93647 - $15.00 USD Received 10 Mar 2008; revised 3 Jun 2008; accepted 3 Jun 2008; published 5 Jun 2008

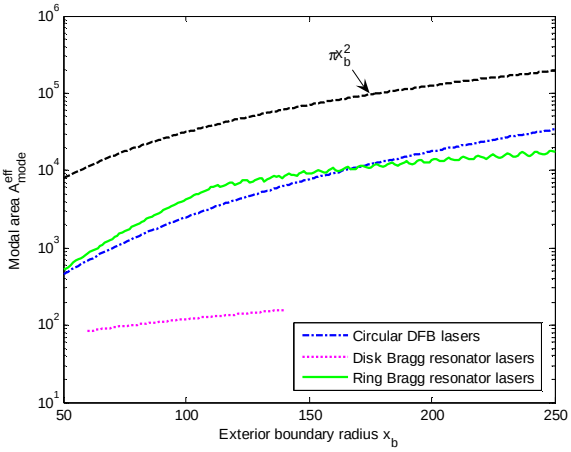

Fig. 7. Modal areas of circular DFB, disk-, and ring- Bragg resonator lasers. Their top surface area (πx_b^2) is marked with a black dashed line as a reference.

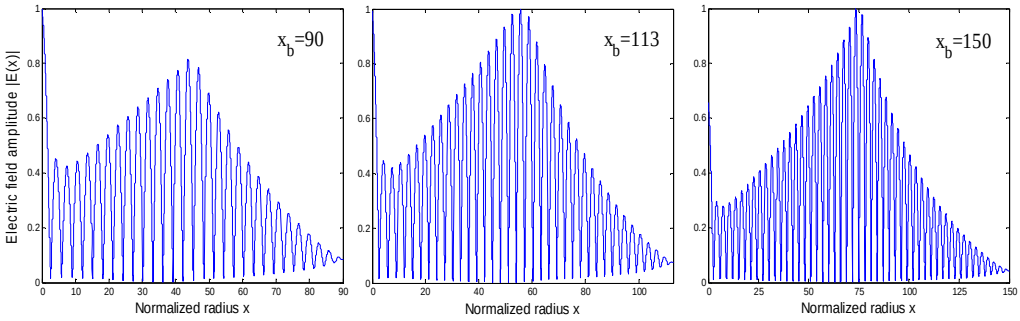

Fig. 8. Comparison of radial electric field profiles of ring Bragg resonator lasers (x_b=90, 113, and 150). For x_b=113, the electric field has equal amplitude at the center (x=0) and the defect (x=x_b/2).

5. Summary

A unified theory for solving and comparing modal properties of surface-emitting chirped circular grating lasers was developed and presented. First, the two types of reflectivities were obtained from the chirped circular gratings under two typical boundary conditions. The asymmetry in the spectra of the reflectivites shows evidence of modal selection due to the involvement of the vertical radiation. Deriving the resonance conditions, the threshold gains and frequency detuning factors of three types of circular grating lasers – circular DFB, disk-, and ring- Bragg resonator lasers, were acquired. This resonance condition theory agrees with previous published results based on characteristic equations. The single mode range, quality factor, emission efficiency, and modal area of these circular grating lasers were studied. A comparison of these metrics concluded that disk Bragg resonator lasers are most useful in low-threshold, high-efficiency, ultracompact laser design, while ring Bragg resonator lasers are excellent candidates for high-efficiency, high-power, large-area lasers.

Acknowledgment

This work was supported in part by the Defense Advanced Research Projects Agency (DARPA) and in part by the National Science Foundation. X. Sun is grateful to J. Sendowski for his kind help in paper revision.

#93647 - $15.00 USD Received 10 Mar 2008; revised 3 Jun 2008; accepted 3 Jun 2008; published 5 Jun 2008